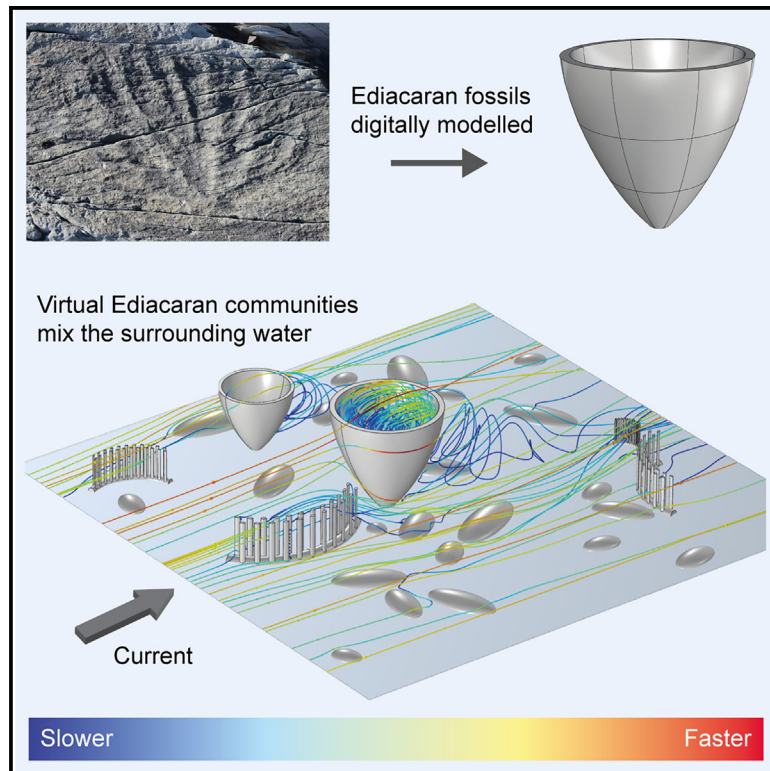


# Current Biology

## Ediacaran marine animal forests and the ventilation of the oceans

### Graphical abstract



### Authors

Susana Gutarra, Emily G. Mitchell, Frances S. Dunn, Brandt M. Gibson, Rachel A. Racicot, Simon A.F. Darroch, Imran A. Rahman

### Correspondence

imran.rahman@nhm.ac.uk

### In brief

Gutarra et al. use computer simulations of water flow to investigate the hydrodynamics of Ediacaran marine animal forests. The results reveal that some Ediacaran communities generated strong patterns of fluid mixing, which could have promoted gas and nutrient transport and thereby enhanced local oxygen concentrations.

### Highlights

- Ediacaran communities were capable of strongly mixing the surrounding water
- Organism shape and size had the greatest influence on mixing patterns
- Mixing could have influenced the distribution of water column resources like oxygen
- Ediacaran communities may have contributed to the ventilation of the oceans



Report

# Ediacaran marine animal forests and the ventilation of the oceans

Susana Gutarra,<sup>1</sup> Emily G. Mitchell,<sup>2</sup> Frances S. Dunn,<sup>3</sup> Brandt M. Gibson,<sup>4,5</sup> Rachel A. Racicot,<sup>6</sup> Simon A.F. Darroch,<sup>6</sup> and Imran A. Rahman<sup>1,3,7,8,\*</sup>

<sup>1</sup>The Natural History Museum, London SW7 5BD, UK

<sup>2</sup>Department of Zoology, University Museum of Zoology Cambridge, University of Cambridge, Cambridge CB2 3EJ, UK

<sup>3</sup>Oxford University Museum of Natural History, University of Oxford, Oxford OX1 3PW, UK

<sup>4</sup>Department of Chemical and Physical Sciences, University of Toronto Mississauga, Mississauga, ON L5L 1C6, Canada

<sup>5</sup>Department of Earth and Environmental Sciences, Vanderbilt University, Nashville, TN 37240, USA

<sup>6</sup>Senckenberg Museum of Natural History, 60325 Frankfurt, Germany

<sup>7</sup>X (formerly Twitter): @VirtualPalaeo

<sup>8</sup>Lead contact

\*Correspondence: [imran.rahman@nhm.ac.uk](mailto:imran.rahman@nhm.ac.uk)

<https://doi.org/10.1016/j.cub.2024.04.059>

## SUMMARY

The rise of animals across the Ediacaran–Cambrian transition marked a step-change in the history of life, from a microbially dominated world to the complex macroscopic biosphere we see today.<sup>1–3</sup> While the importance of bioturbation and swimming in altering the structure and function of Earth systems is well established,<sup>4–6</sup> the influence of epifaunal animals on the hydrodynamics of marine environments is not well understood. Of particular interest are the oldest “marine animal forests,”<sup>7</sup> which comprise a diversity of sessile soft-bodied organisms dominated by the fractally branching rangeomorphs.<sup>8,9</sup> Typified by fossil assemblages from the Ediacaran of Mistaken Point, Newfoundland,<sup>8,10,11</sup> these ancient communities might have played a pivotal role in structuring marine environments, similar to modern ecosystems,<sup>7,12,13</sup> but our understanding of how they impacted fluid flow in the water column is limited. Here, we use ecological modeling and computational flow simulations to explore how Ediacaran marine animal forests influenced their surrounding environment. Our results reveal how organism morphology and community structure and composition combined to impact vertical mixing of the surrounding water. We find that Mistaken Point communities were capable of generating high-mixing conditions, thereby likely promoting gas and nutrient transport within the “canopy.” This mixing could have served to enhance local-scale oxygen concentrations and redistribute resources like dissolved organic carbon. Our work suggests that Ediacaran marine animal forests may have contributed to the ventilation of the oceans over 560 million years ago, well before the Cambrian explosion of animals.

## RESULTS

Here, we use large-scale flow simulations to study the hydrodynamic effects of Ediacaran marine forests, illuminating their potential role in controlling the distribution of water column resources and influencing the late Neoproterozoic rise of animals. We analyzed three Mistaken Point bedding planes (~565 Ma<sup>11</sup>), which consist of assemblages of sessile marine organisms preserved *in situ*.<sup>8,14–16</sup> We simulated five communities for each surface, with the identity, size, and spacing of fossils based on known spatial patterns,<sup>9,16–18</sup> using the R package spatstat.<sup>19</sup> We then created three-dimensional digital models of the principal taxa using computer-aided design software (Figure S1A) and arranged them to reflect the composition and structure of the simulated communities (Figure S1B). Computational fluid dynamics (CFD) simulations were used to investigate the hydrodynamics of these virtual communities under a range of current velocities informed by the sedimentological characteristics of the bedding surfaces<sup>14</sup> and data recorded for analogous modern deep-sea settings.<sup>20,21</sup>

Our simulations demonstrate that Ediacaran marine animal forests were capable of influencing their fluid environment, with the “D,” “E,” and Lower Mistaken Point (LMP) surfaces producing substantially different patterns of fluid flow (Figures 1, 2, and S2). In the D surface communities, the wakes of upright organisms had wider areas of influence, with greater interaction between them (Figures 1 and S2A), compared to the other two surfaces. In contrast, upright organisms in the E surface communities created smaller and sparser wakes, with very little interaction, while the LMP surface communities showed an intermediate pattern (Figures 1 and S2A). The mean streamwise velocity ( $u/U_0$ ) profiles from the D surface community simulations displayed an inflection point and a roughness layer where the flow was slowed (Figure S2B), characteristics of canopy flow.<sup>7,22</sup> These velocity profiles were noticeably different from an undisturbed boundary layer flow profile (logarithmic-shaped, formed in the absence of canopy).<sup>23</sup> In contrast, the E surface community velocity profiles were much closer to an undisturbed boundary layer flow, with no clear inflection point (Figure S2B). The LMP surface community profiles showed an



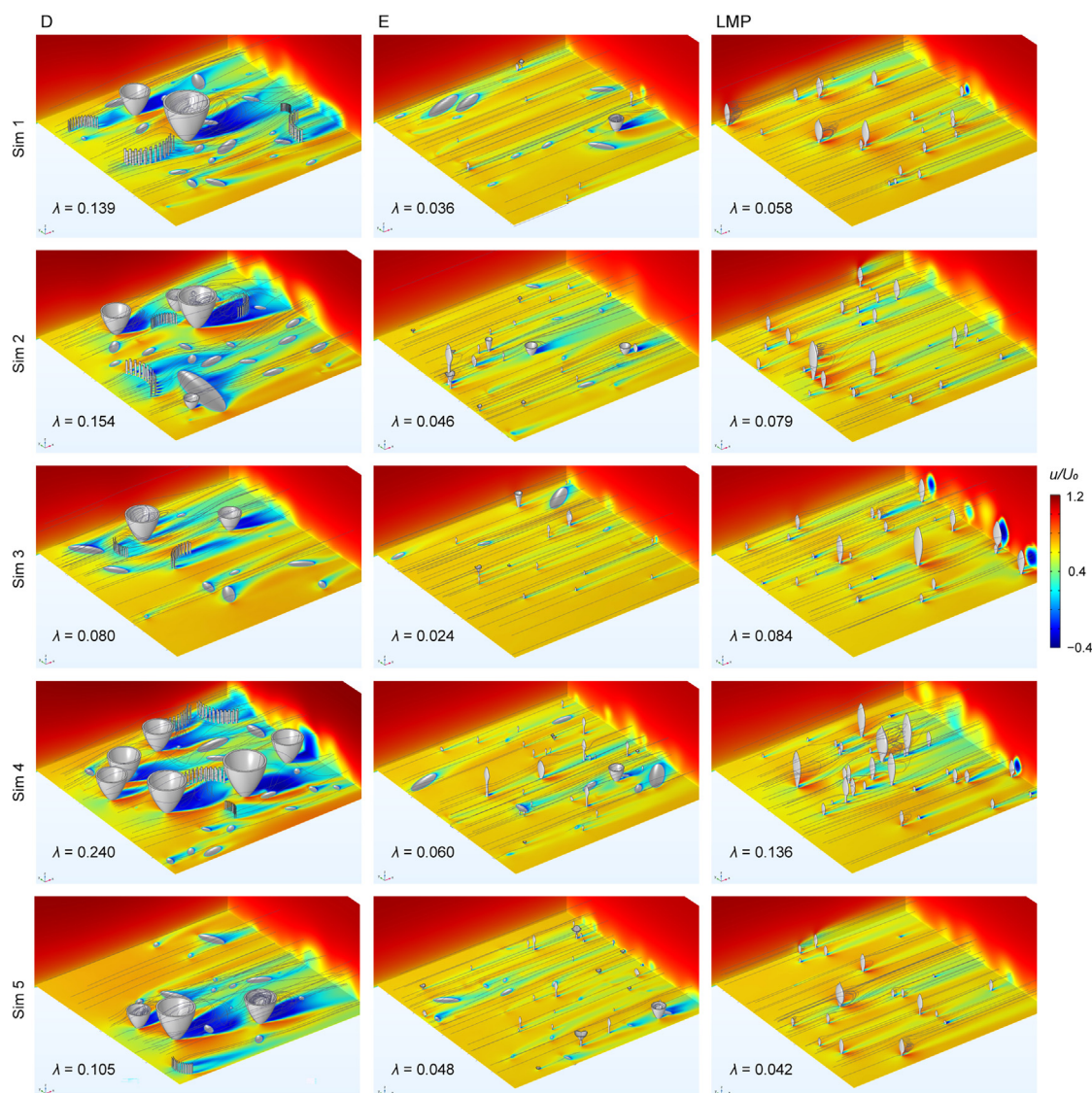


**Figure 1. Streamwise velocity patterns for virtual communities of three Mistaken Point assemblages**

Oblique views of CFD simulations for five simulated communities (Sim 1–Sim 5) of the D, E, and LMP surfaces (1 m<sup>2</sup> area), showing organisms in 3D, flow streamlines (gray lines), and two-dimensional plots of the streamwise velocity (at height  $z = 1$  cm in the horizontal plane and two vertical planes at the side and back of the domain). The streamwise velocity ( $u$ ) has been normalized to the inlet velocity ( $U_0 = 0.1 \text{ m s}^{-1}$ ). The frontal area index ( $\lambda$ ), representing the element planform area per unit of community area, is shown for each simulation. Direction of ambient flow from left to right.

See also [Figures S1–S3](#).

intermediate pattern between the D and E surface communities ([Figure S2B](#)).

CFD results show that vertical mixing was greatly enhanced for the D surface communities ([Figures 2 and 3](#)). Simulations of this surface displayed stronger perturbations of vertical velocity ( $w/U_0$ ) compared to the E and LMP surfaces, both close to the bottom and higher in the water column ([Figures 2 and 3](#)). Vertical velocity plots had a characteristic “bottle” shape ([Figure 3](#)), with the greatest spread of vertical velocity occurring between 5 and 10 cm above the seafloor. In contrast, vertical velocity plots were narrowest for the E surface communities, similar to the results obtained from our simulation of an idealized modern marine animal forest

([Figures S3A–S3C](#)) and indicative of restricted vertical mixing, whereas they showed an intermediate spread of values for the LMP surface communities ([Figure 3](#)). Additionally, vertical mixing extended higher into the water column for the D and LMP surface communities compared to the E surface communities ([Figure 3](#)). Similar to vertical mixing, lateral mixing was enhanced for the D surface communities, restricted for the E surface communities, and intermediate for the LMP surface communities, as shown by the plots of lateral velocity ( $v/U_0$ ) ([Figures S2C and S2D](#)). These described flow patterns, based on simulated communities, were consistent with results from real quadrants randomly selected from previously compiled datasets<sup>8,17</sup> ([Figures S3D–S3F](#)). This



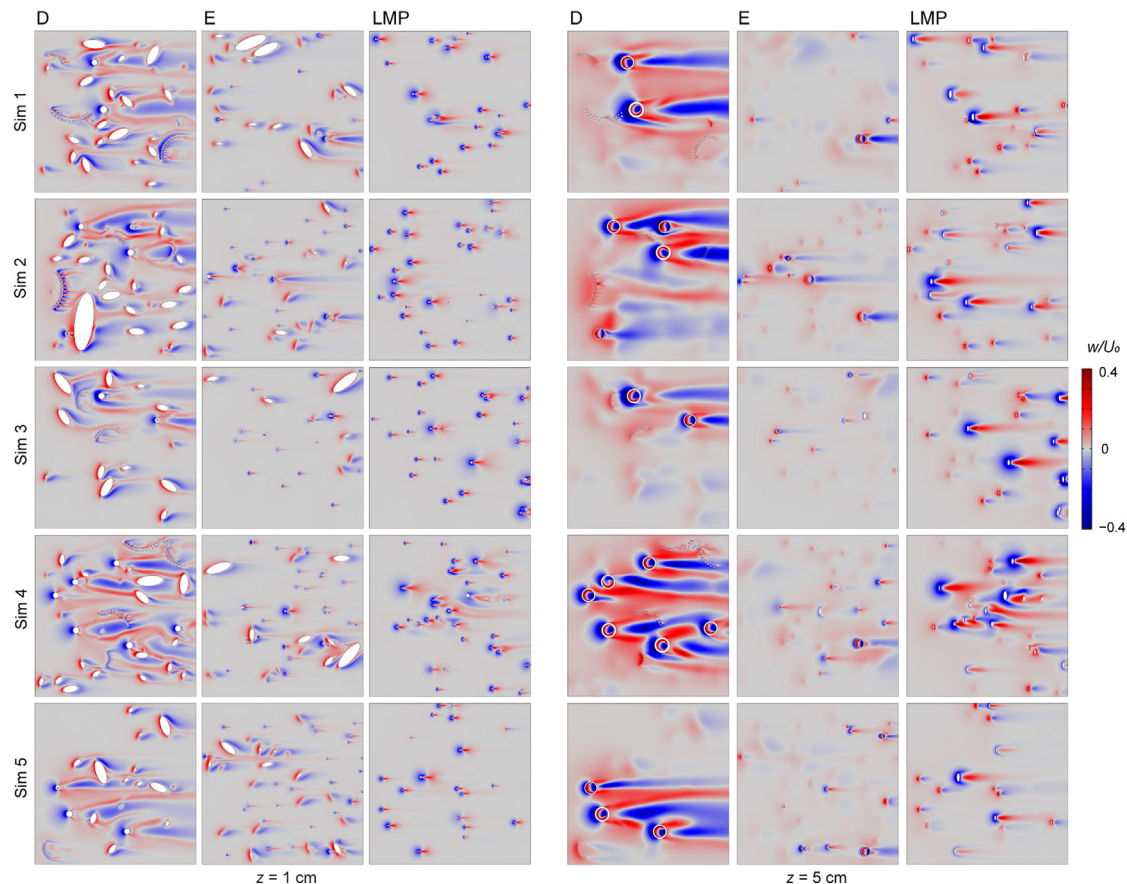


**Figure 2. Vertical velocity patterns for virtual communities of three Mistaken Point assemblages**

CFD results for five simulated communities (Sim 1–Sim 5) of the D, E, and LMP surfaces. Two-dimensional plots of vertical velocity ( $w$ ) relative to the inlet velocity ( $U_0 = 0.1 \text{ m s}^{-1}$ ) for two horizontal cross-sections at heights  $z = 1 \text{ cm}$  (left panels) and  $z = 5 \text{ cm}$  (right panels). Direction of ambient flow from left to right. See also [Figures S1–S3](#).

relative ordering remained consistent across the full range of simulated current velocities (0.01, 0.05, 0.1, and 0.2 m/s). Additionally, the variance of vertical and lateral velocities (represented by the standard deviation of these two velocity components) was significantly higher for the D surface communities compared to the E and LMP surface communities (Welch's two-sample t test for unequal variance; D surface communities versus E surface communities,  $p = 0.0051$ ; D surface communities versus LMP surface communities,  $p = 0.0022$ ; [Figures 4A and 4B](#); [Table S1](#)), as well as for the LMP surface communities compared to the E surface communities ( $p = 0.0229$ ; [Table S1](#)). The frontal area index ( $\lambda$ ), a metric indicative of canopy density,<sup>7,24</sup> mirrored these trends in vertical and lateral mixing, being lowest for the E surface communities, intermediate for the LMP surface communities, and highest for the D surface communities ([Figures 1 and 4C](#); [Table S2](#)). Other calculated parameters such as the total and average height of the canopy and the extent of tiering (i.e., distinct vertical stratification metric based on total height<sup>18</sup>) were not closely correlated with vertical or lateral mixing ([Figures 4D–4F](#); [Table S2](#)).

The large, bluff-shaped rangeomorph *Bradgatia* exerted the strongest influence on flow in the D surface communities ([Figures 1 and S2A](#)). It was the main contributor to patterns of vertical and lateral mixing, accounting for an average of 56% of  $\lambda$  ([Table S2](#))

despite *Fractofusus* being the dominant taxon on this surface. The D surface community *Bradgatia* individuals created broad wakes, with strong recirculation ([Figures 1 and S2A](#)), flow acceleration at the wake margins ([Figures 1 and S2A](#)), and areas of highly positive and negative vertical and lateral velocity ([Figures 2 and S2C](#)). Our sensitivity tests of different reconstructions of the morphology of *Bradgatia* showed similar patterns ([Figure S4](#)). The LMP surface communities, which had the second strongest patterns of mixing, were dominated by frondose forms and were characterized by the tallest specimens of all three surfaces in terms of both maximum and average specimen heights ([Figures 4D and 4E](#); [Table S2](#)). In the LMP surface communities, the uniterminal frond *Beothukis* was typically the main contributor to mixing (making up an average of 55% of  $\lambda$ ; [Table S2](#)). Velocity plots showed that tall fronds could strongly influence flow patterns around them ([Figures 1 and S2A](#)). Their wakes were not as broad as those observed for *Bradgatia* from the D surface communities, but they still produced substantial recirculation ([Figures 1 and S2A](#)) and were effective in diverting the flow both vertically ([Figure 2](#)) and laterally ([Figure S2C](#)). The main contributors to  $\lambda$  in the E surface communities were *Fractofusus* and *Charniodiscus* ([Table S2](#)), which did not reach heights above the sediment-water interface comparable to fronds from the D and LMP surface



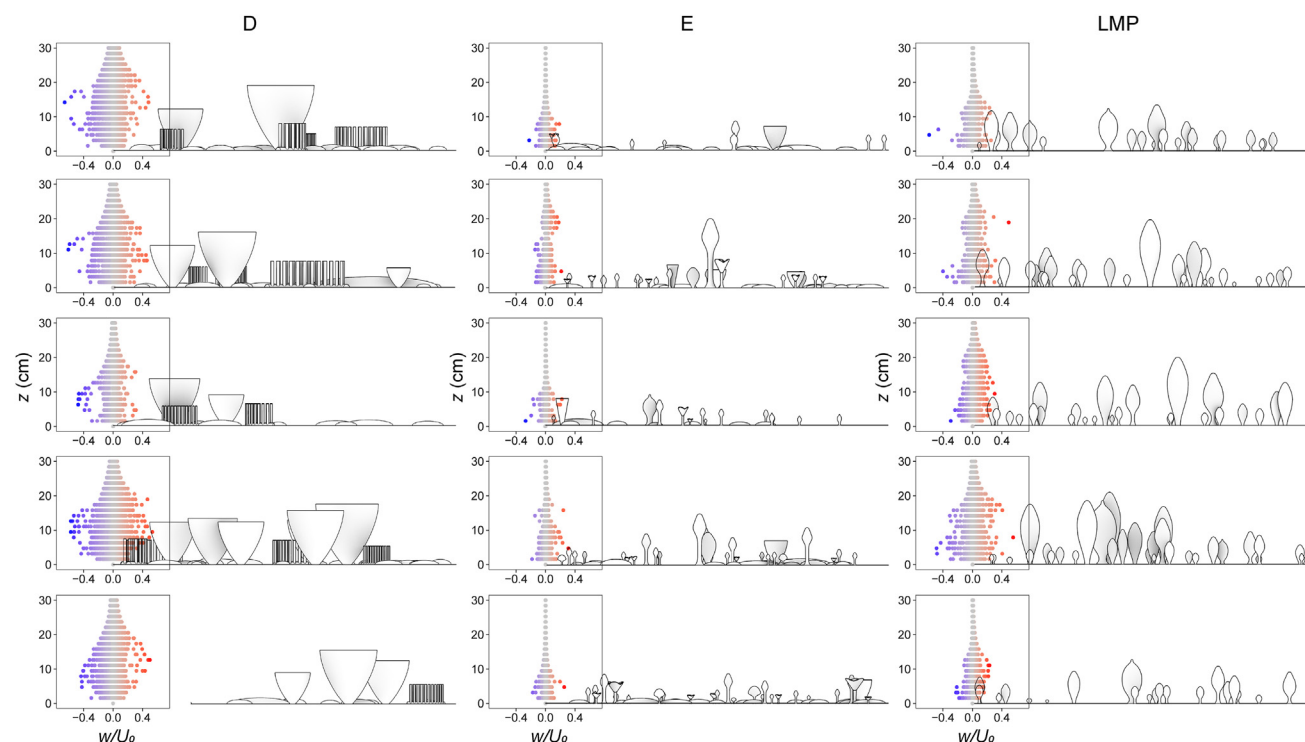


**Figure 3. Dispersion of vertical velocity for virtual communities of three Mistaken Point assemblages**

Plots of vertical velocity ( $w$ ) relative to the inlet velocity ( $U_0 = 0.1 \text{ m s}^{-1}$ ) for five simulated communities of the D, E, and LMP surfaces at heights between  $z = 0$  and  $z = 30 \text{ cm}$ , with organism profiles (frontal views) scaled to  $z$ . Vertical velocities were sampled from a grid of  $20 \times 20 \times 20$  points in  $x$ ,  $y$ , and  $z$  directions over the  $1 \text{ m}^2$  community. Positive velocities (upward direction) are represented in red and negative velocities (downward direction) in blue.

See also [Figures S1](#) and [S3](#).

communities ([Figures 1](#) and [3](#)). Additionally, taxa with bluff morphologies (i.e., *Bradgatia* and *Thectardis*) were less abundant and smaller in the E surface communities.

Next, we tested the influence of size and morphology on the observed flow patterns by creating hypothetical communities based on the D surface. Sensitivity analyses where *Bradgatia* individuals were re-sized to match the height distribution of this taxon in the E surface communities confirmed that morphology had an important influence on the CFD results, but only in the context of sufficiently large sizes. Reducing the size of *Bradgatia* decreased  $\lambda$  and resulted in smaller wakes, attenuated canopy flow patterns, and weaker vertical and lateral mixing, comparable to results seen for the LMP surface communities ([Figure S4](#)). In another suite of simulations, we replaced *Bradgatia* with the uniterminal frond *Beothukis*, thereby keeping the maximum height, average height, and tiering unchanged, while reducing  $\lambda$ . This change in morphology had a strong effect on the velocity patterns, resulting in smaller wakes, attenuated roughness layer and canopy flow effects, and a narrower spread of vertical and lateral velocities ([Figure S4](#)), indicating that tiering alone was not sufficient to generate strong mixing.  $\lambda$  better summarizes the influence of multiple aspects (i.e., organism abundance, morphology, and size). Our results show that the relative abundance of organisms did not play a key role in governing flow patterns of Mistaken Point communities, as illustrated by the fact that the densest community found on the E surface was also the one with the weakest mixing ([Table S2](#)). Instead, mixing

patterns were highly dependent on shape, but this effect was also modulated by size. The strongest patterns were created by large bulbous shapes (e.g., *Bradgatia* in the D surface communities), followed by tall and broad sail-like morphologies (e.g., uniterminal fronds in the LMP surface communities) ([Figures 1](#) and [S2A](#)).

## DISCUSSION

We find that Ediacaran communities had the potential to create high-mixing conditions. Vertical mixing of water is known to be a key process in modern oceans, serving to redistribute heat, nutrients, and larvae,<sup>25</sup> as well as more broadly affecting ocean stratification and the energy cascade.<sup>26</sup> Moreover, modern marine animal forests have been shown to alter turbulent mixing and the exchange of dissolved and particulate substances within and above the canopy.<sup>7</sup> The deep-water environment inhabited by the Mistaken Point biota is thought to have been oxic with low concentrations of organic carbon.<sup>27,28</sup> Locally enhanced vertical and lateral mixing created by Ediacaran marine animal forests, as revealed by our analyses, could thus have had a major impact on resource distribution. Intermediate-to-dense canopy regimes, such as those described for the D and LMP surface communities, would be expected to have increased near-bed turbulence and promoted gas and nutrient transport within the canopy.<sup>7</sup> Such regimes might have brought about conspicuous changes to Ediacaran deep marine environments, including

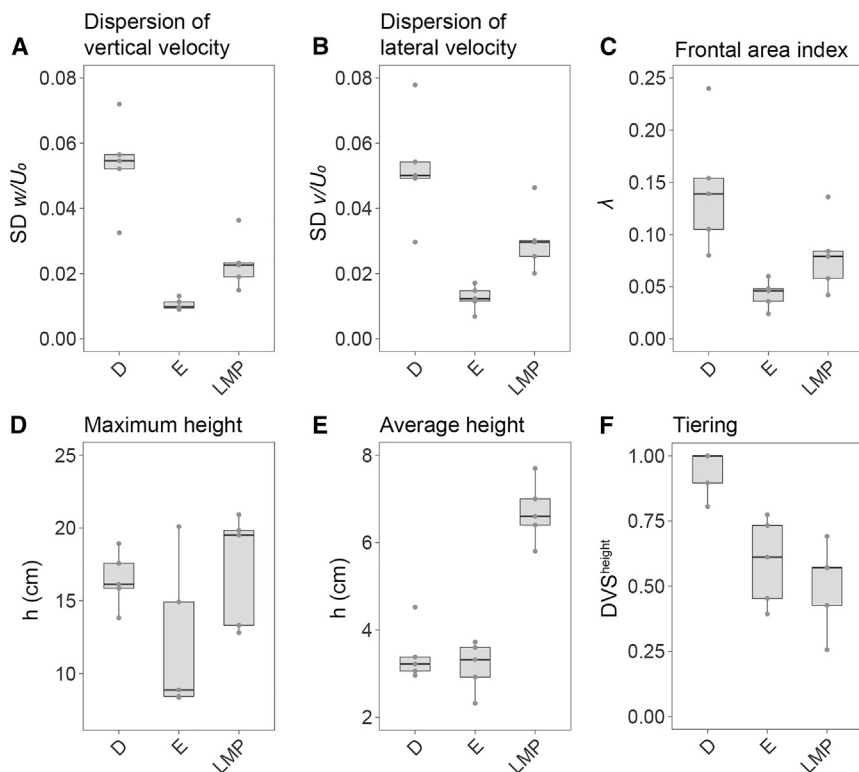


**Figure 4. Comparison of vertical and lateral velocity dispersion and geometrical parameters for five simulated communities of the D, E, and LMP surfaces**

(A and B) Standard deviation (SD) of the vertical (A) and lateral (B) velocity components ( $w$  and  $v$ , respectively), normalized to the inlet velocity,  $U_0 = 0.1 \text{ m s}^{-1}$ .

(C) Frontal area index ( $\lambda$ ) calculated as the element planform area per unit of community area.

(D) Maximum height ( $h$ ) represented by the height of the tallest organism in each  $1 \text{ m}^2$  virtual community.

(E) Average height ( $h$ ) calculated as the average height of all organisms in each  $1 \text{ m}^2$  virtual community.

(F) Tiering metric, indicating the degree of distinct vertical stratification based on total height ( $DVS^{height}$ ). Boxplots display individual values (gray points), median (black line), and interquartile range (gray box).

See also [Figure S4](#) and [Tables S1](#) and [S2](#).

oxygenation of the water column and the redistribution of dissolved organic carbon.

The strong mixing created by some Mistaken Point communities is suggestive of a previously unrecognized positive and synecological feedback that could have promoted the ventilation of benthic marine environments in the late Neoproterozoic. The Ediacaran was associated with profound shifts in ocean chemistry, sediment redox gradients, and the structure of global biogeochemical cycles.<sup>27–30</sup> Long episodes of anoxia were punctuated by short pulses of oxygenation,<sup>29,31</sup> with the appearance of abundant and diverse macroscopic organisms from  $\sim 574 \text{ Ma}$ <sup>11</sup> roughly coinciding with the Shuram carbon isotope excursion  $\sim 574\text{--}567 \text{ Ma}$ <sup>30,32</sup> (which might be linked to an extensive oxygenation event<sup>33,34</sup>). In this context, the promotion of vertical mixing by Ediacaran marine forests could have played a crucial role in enhancing local oxygen concentrations. Moreover, increased biological mixing by early animals (including the first marine animal forests) might have driven a rise in oxygen by reducing the concentration of suspended organic carbon in the water, thereby ensuring a well-ventilated environment.<sup>4,6</sup>

These results are consistent with emerging reinterpretations of Ediacaran paleobiology. The frondose rangeomorphs, which dominate Mistaken Point surfaces,<sup>8,9</sup> exhibited high surface area-to-volume (SA:V) ratios due to their branching architecture.<sup>35,36</sup> Although previously inferred to be an adaptation for feeding by absorbing dissolved organic carbon (i.e., osmotrophy),<sup>35,37</sup> recent work has suggested this might not be feasible due to the difficulties associated with external digestion of recalcitrant organic matter in environments characterized by persistent currents.<sup>38,39</sup> However, an alternative interpretation of rangeomorph fronds as respiratory structures may be more

plausible as this would benefit from exposure to high-energy currents and the associated reduction in the thickness of the diffusive boundary layer, which would have served to enhance the transmission of gases across frond surfaces.<sup>39,40</sup>

Consequently, the high SA:V ratios of rangeomorphs could represent an adaptation for maximizing oxygen uptake.

In summary, our simulations demonstrate that Ediacaran marine forests created complex flow patterns that would have influenced the distribution of resources in the water column, including nutrients and oxygen. In particular, we show that the rangeomorph-dominated Ediacaran communities preserved around the Avalon Peninsula would have enhanced vertical mixing, thereby increasing oceanic ventilation. Our results thus reveal that Earth's earliest animals were capable of substantially modifying their marine environments, similar to present-day communities of benthic invertebrates.<sup>41–43</sup> These changes may have imposed spatial anisotropies on Ediacaran ecosystems tens of millions of years prior to the Cambrian explosion, providing support for recent suggestions that habitat heterogeneity was crucial for the emergence of motile eumetazoans and bilaterians.<sup>44,45</sup> Ventilation by marine forests therefore could have played an important role in shaping late Neoproterozoic marine environments and enabling the rise of animals.

## STAR★METHODS

Detailed methods are provided in the online version of this paper and include the following:

- [KEY RESOURCES TABLE](#)
- [RESOURCE AVAILABILITY](#)
  - Lead contact
  - Materials availability
  - Data and code availability
- [EXPERIMENTAL MODEL AND SUBJECT DETAILS](#)
  - Material
- [METHOD DETAILS](#)

- Digital modeling of virtual communities
- Computational fluid dynamics
- Sensitivity tests
- **QUANTIFICATION AND STATISTICAL ANALYSIS**

### SUPPLEMENTAL INFORMATION

Supplemental information can be found online at <https://doi.org/10.1016/j.cub.2024.04.059>.

### ACKNOWLEDGMENTS

This research was supported by joint funding from the UK Natural Environment Research Council (NE/V010859/2) and the US National Science Foundation (NSF-NERC EAR-2007928) to I.A.R. and S.A.F.D. E.G.M. also acknowledges funding from the Natural Environment Research Council (NE/S014756/1). F.S.D. acknowledges support from the Royal Commission for the Exhibition of 1851, Merton College, Oxford, and the Natural Environment Research Council (NE/W00786X/1). B.M.G. acknowledges computational support stemming from two Vanderbilt University Alberstadt, Reeseman, and Sterns grants and a University of Toronto Mississauga Postdoctoral Fellowship. S.A.F.D. and R.A.R. acknowledge generous support from the Alexander von Humboldt Foundation, which is sponsored by the Federal Ministry for Education and Research in Germany. We are grateful to Jim Schiffbauer and an anonymous reviewer for comments on an earlier version of the manuscript.

### AUTHOR CONTRIBUTIONS

Conceptualization, I.A.R., S.A.F.D., F.S.D., B.M.G., and R.A.R.; methodology, S.G. and E.G.M.; formal analysis, S.G. and E.G.M.; data curation, S.G. and I.A.R.; writing – original draft, S.G. and I.A.R.; writing – review & editing, I.A.R., E.G.M., S.A.F.D., F.S.D., S.G., B.M.G., and R.A.R.; visualization, S.G.; supervision, I.A.R. and S.A.F.D.; project administration, I.A.R. and S.A.F.D.; funding acquisition, I.A.R., S.A.F.D., F.S.D., B.M.G., and R.A.R.

### DECLARATION OF INTERESTS

The authors declare no competing interests.

Received: December 8, 2023

Revised: March 18, 2024

Accepted: April 25, 2024

Published: May 17, 2024

### REFERENCES

- Erwin, D.H., Laflamme, M., Tweedt, S.M., Sperling, E.A., Pisani, D., and Peterson, K.J. (2011). The Cambrian Conundrum: early divergence and later ecological success in the early history of animals. *Science* 334, 1091–1097.
- Droser, M.L., and Gehling, J.G. (2015). The advent of animals: the view from the Ediacaran. *Proc. Natl. Acad. Sci. USA* 112, 4865–4870.
- Droser, M.L., Tarhan, L.G., and Gehling, J.G. (2017). The rise of animals in a changing environment: global ecological innovation in the Late Ediacaran. *Annu. Rev. Earth Planet Sci.* 45, 593–617.
- Butterfield, N.J. (2009). Oxygen, animals and oceanic ventilation: an alternative view. *Geobiology* 7, 1–7.
- Canfield, D.E., and Farquhar, J. (2009). Animal evolution, bioturbation, and the sulfate concentration of the oceans. *Proc. Natl. Acad. Sci. USA* 106, 8123–8127.
- Butterfield, N.J. (2018). Oxygen, animals and aquatic bioturbation: an updated account. *Geobiology* 16, 3–16.
- Guizien, K., and Ghisalberti, M. (2017). Living in the canopy of the animal forest: physical and biogeochemical aspects. In *Marine Animal Forests*, S. Rossi, ed. (Springer), pp. 507–528.
- Clapham, M.E., Narbonne, G.M., and Gehling, J.G. (2003). Paleoeology of the oldest known animal communities: Ediacaran assemblages at Mistaken Point, Newfoundland. *Paleobiology* 29, 527–544.
- Mitchell, E.G., Harris, S., Kenchington, C.G., Vixseboxse, P., Roberts, L., Clark, C., Dennis, A., Liu, A.G., and Wilby, P.R. (2019). The importance of neutral over niche processes in structuring Ediacaran early animal communities. *Ecol. Lett.* 22, 2028–2038.
- Ghisalberti, M., Gold, D.A., Laflamme, M., Clapham, M.E., Narbonne, G.M., Summons, R.E., Johnston, D.T., and Jacobs, D.K. (2014). Canopy flow analysis reveals the advantage of size in the oldest communities of multicellular eukaryotes. *Curr. Biol.* 24, 305–309.
- Matthews, J.J., Liu, A.G., Yang, C., McIlroy, D., Levell, B., and Condon, D.J. (2021). A chronostratigraphic framework for the rise of the Ediacaran macrobiota: new constraints from Mistaken Point Ecological Reserve, Newfoundland. *Geol. Soc. Am. Bull.* 133, 612–624.
- Rossi, S. (2013). The destruction of the ‘animal forests’ in the oceans: towards an oversimplification of the benthic ecosystems. *Ocean Coast Manag.* 84, 77–85.
- Rossi, S., Bramanti, L., Gori, A., and Covadonga, O. (2017). Animal forests of the world: an overview. In *Marine Animal Forests*, S. Rossi, ed. (Springer), pp. 1–28.
- Wood, D.A., Dalrymple, R.W., Narbonne, G.M., Gehling, J.G., and Clapham, M.E. (2003). Paleoenvironmental analysis of the late Neoproterozoic Mistaken Point and Trepassy formations, southeastern Newfoundland. *Can. J. Earth Sci.* 40, 1375–1391.
- Darroch, S.A.F., Laflamme, M., and Clapham, M.E. (2013). Population structure of the oldest known macroscopic communities from Mistaken Point, Newfoundland. *Paleobiology* 39, 591–608.
- Mitchell, E.G., and Butterfield, N.J. (2018). Spatial analyses of Ediacaran communities at Mistaken Point. *Paleobiology* 44, 40–57.
- Mitchell, E.G., Kenchington, C.G., Liu, A.G., Matthews, J.J., and Butterfield, N.J. (2015). Reconstructing the reproductive mode of an Ediacaran macro-organism. *Nature* 524, 343–346.
- Mitchell, E.G., and Kenchington, C.G. (2018). The utility of height for the Ediacaran organisms of Mistaken Point. *Nat. Ecol. Evol.* 2, 1218–1222.
- Baddeley, A., Rubak, E., and Turner, R. (2015). Spatial point patterns. *Methodology and Applications with R* (Chapman & Hall/CRC).
- Zimmerman, H.B. (1971). Bottom currents on the New England continental rise. *J. Geophys. Res.* 76, 5865–5876.
- Richardson, P.L. (1985). Average velocity and transport of the Gulf Stream near 55W. *J. Mar. Res.* 43, 83–111.
- Brunet, Y. (2020). Turbulent flow in plant canopies: historical perspective and overview. *Bound.-Layer Meteorol.* 177, 315–364.
- Schlichting, H., and Gersten, K. (2000). *Boundary-Layer Theory* (Springer).
- Nepf, H., Lightbody, A., and Ghisalberti, M. (2007). Transport in aquatic canopies. In *Flow and Transport Processes with Complex Obstructions*, A.G. Yevgeny, and J.C.R. Hunt, eds. (Springer), pp. 221–250.
- Robertson, R., and Dong, C. (2019). An evaluation of the performance of vertical mixing parameterizations for tidal mixing in the Regional Ocean Modeling System (ROMS). *Geosci. Lett.* 6, 15.
- Munk, W., and Wunsch, C. (1998). Abyssal recipes II: energetics of tidal and wind mixing. *Deep-Sea Res. Part I Oceanogr. Res. Pap.* 45, 1977–2010.
- Canfield, D.E., Poulton, S.W., and Narbonne, G.M. (2007). Late-Neoproterozoic deep-ocean oxygenation and the rise of animal life. *Science* 315, 92–95.
- Bowyer, F., Wood, R.A., and Poulton, S.W. (2017). Controls on the evolution of Ediacaran metazoan ecosystems: a redox perspective. *Geobiology* 15, 516–551.
- Sahoo, S.K., Planavsky, N.J., Jiang, G., Kendall, B., Owens, J.D., Wang, X., Shi, X., Anbar, A.D., and Lyons, T.W. (2016). Oceanic oxygenation events in the anoxic Ediacaran ocean. *Geobiology* 14, 457–468.
- Rooney, A.D., Cantine, M.D., Bergmann, K.D., Gómez-Pérez, I., Al Baloushi, B., Boag, T.H., Busch, J.F., Sperling, E.A., and Strauss, J.V. (2020).



- Calibrating the coevolution of Ediacaran life and environment. *Proc. Natl. Acad. Sci. USA* **117**, 16824–16830.
31. Kendall, B., Komiya, T., Lyons, T.W., Bates, S.M., Gordon, G.W., Romaniello, S.J., Jiang, G., Creaser, R.A., Xiao, S., McFadden, K., et al. (2015). Uranium and molybdenum isotope evidence for an episode of widespread ocean oxygenation during the late Ediacaran Period. *Geochim. Cosmochim. Acta* **156**, 173–193.
32. Yang, C., Rooney, A.D., Condon, D.J., Li, X.-H., Grazhdankin, D.V., Bowyer, F.T., Hu, C., Macdonald, F.A., and Zhu, M. (2021). The tempo of Ediacaran evolution. *Sci. Adv.* **7**, eabi9643.
33. Fike, D.A., Grotzinger, J.P., Pratt, L.M., and Summons, R.E. (2006). Oxidation of the Ediacaran ocean. *Nature* **444**, 744–747.
34. Zhang, F., Xiao, S., Romaniello, S.J., Hardisty, D., Li, C., Melezhik, V., Pokrovsky, B., Cheng, M., Shi, W., Lenton, T.M., and Anbar, A.D. (2019). Global marine redox changes drove the rise and fall of the Ediacara biota. *Geobiology* **17**, 594–610.
35. Laflamme, M., Xiao, S., and Kowalewski, M. (2009). Osmotrophy in modular Ediacara organisms. *Proc. Natl. Acad. Sci. USA* **106**, 14438–14443.
36. Hoyal Cuthill, J.F., and Conway Morris, S. (2014). Fractal branching organizations of Ediacaran rangeomorph fronds reveal a lost Proterozoic body plan. *Proc. Natl. Acad. Sci. USA* **111**, 13122–13126.
37. Laflamme, M., Darroch, S.A., Tweedt, S.M., Peterson, K.J., and Erwin, D.H. (2013). The end of the Ediacara biota: extinction, biotic replacement, or Cheshire cat? *Gondwana Res.* **23**, 558–573.
38. Liu, A.G., Kenchington, C.G., and Mitchell, E.G. (2015). Remarkable insights into the paleoecology of the Avalonian Ediacaran macrobiota. *Gondwana Res.* **27**, 1355–1380.
39. Butterfield, N.J. (2022). Constructional and functional anatomy of Ediacaran rangeomorphs. *Geol. Mag.* **159**, 1148–1159.
40. Darroch, S.A.F., Gutarra, S., Masaki, H., Olaru, A., Gibson, B.M., Dunn, F.S., Mitchell, E.G., Racicot, R.A., Burzynski, G., and Rahman, I.A. (2023). The rangeomorph *Pectinifrons abyssalis*: hydrodynamic function at the dawn of animal life. *iScience* **26**, 105989.
41. Gili, J.-M., and Coma, R. (1998). Benthic suspension feeders: their paramount role in littoral marine food webs. *Trends Ecol. Evol.* **13**, 316–321.
42. de Smit, J.C., Brückner, M.Z.M., Mesdag, K.I., Kleinhans, M.G., and Bouma, T.J. (2021). Key bioturbator species within benthic communities determine sediment resuspension thresholds. *Front. Mar. Sci.* **8**, 726238.
43. Jørgensen, B.B., Wenzhöfer, F., Egger, M., and Glud, R.N. (2022). Sediment oxygen consumption: role in the global marine carbon cycle. *Earth Sci. Rev.* **228**, 103987.
44. Budd, G.E., and Jensen, S. (2017). The origin of the animals and a ‘Savannah’ hypothesis for early bilaterian evolution. *Biol. Rev.* **92**, 446–473.
45. Mussini, G., and Dunn, F.S. (2024). Decline and fall of the Ediacarans: late-Neoproterozoic extinctions and the rise of the modern biosphere. *Biol. Rev.* **99**, 110–130.
46. Pomeroy, A.W.M., Ghisalberti, M., Peterson, M., and Farooji, V.E. (2023). A framework to quantify flow through coral reefs of varying coral cover and morphology. *PLoS One* **18**, e0279623.
47. R Core Team (2023). R: a language and environment for statistical computing (R Foundation for Statistical Computing). <https://www.R-project.org>.
48. Ichaso, A.A., Dalrymple, R.W., and Narbonne, G.M. (2007). Paleoenvironmental and basin analysis of the late Neoproterozoic (Ediacaran) upper Conception and St. John’s groups, west Conception Bay, Newfoundland. *Can. J. Earth Sci.* **44**, 25–41.
49. Bamforth, E.L., Narbonne, G.M., and Anderson, M.M. (2008). Growth and ecology of a multi-branched Ediacaran rangeomorph from the Mistaken Point assemblage, Newfoundland. *J. Paleontol.* **82**, 763–777.
50. Gehling, J.G., and Narbonne, G.M. (2007). Spindle-shaped Ediacara fossils from the Mistaken Point assemblage, Avalon Zone, Newfoundland. *Can. J. Earth Sci.* **44**, 367–387.
51. Flude, L.I., and Narbonne, G.M. (2008). Taphonomy and ontogeny of a multibranched Ediacaran fossil: *Bradgatia* from the Avalon Peninsula of Newfoundland. *Can. J. Earth Sci.* **45**, 1095–1109.
52. Kenchington, C.G., and Wilby, P.R. (2017). Rangeomorph classification schemes and intra-specific variation: are all characters created equal? *Geol. Soc. Spec. Publ.* **448**, 221–250.
53. Mason, S.J., and Narbonne, G.M. (2016). Two new Ediacaran small fronds from Mistaken Point, Newfoundland. *J. Paleontol.* **90**, 183–194.
54. Clapham, M.E., Narbonne, G.M., Gehling, J.G., Greentree, C., and Anderson, M.M. (2004). *Thectardis avalonensis*: a new Ediacaran fossil from the Mistaken Point biota, Newfoundland. *J. Paleontol.* **78**, 1031–1036.
55. Laflamme, M., Narbonne, G.M., and Anderson, M.M. (2004). Morphometric analysis of the Ediacaran frond *Charniodiscus* from the Mistaken Point Formation, Newfoundland. *J. Paleontol.* **78**, 827–837.
56. Hawco, J.B., Kenchington, C.G., Taylor, R.S., and McIlroy, D. (2020). A multivariate statistical analysis of the Ediacaran rangeomorph taxa *Beothukis* and *Culmoifrons*. *Palaio* **35**, 495–511.
57. Vixseboxse, P.B., Kenchington, C.G., Dunn, F.S., and Mitchell, E.G. (2021). Orientations of Mistaken Point fronds indicate morphology impacted ability to survive turbulence. *Front. Earth Sci.* **9**, 762824.
58. Stow, D.A., Hernández-Molina, F.J., Llave, E., Sayago-Gil, M., Díaz del Río, V., and Branson, A. (2009). Bedform-velocity matrix: the estimation of bottom current velocity from bedform observations. *Geology* **37**, 327–330.
59. Spalart, P.R., and Allmaras, S.R. (1994). A one-equation turbulence model for aerodynamic flows. *La Rech. Aéropatiale* **1**, 5–21.
60. Gibson, B.M., Darroch, S.A., Maloney, K.M., and Laflamme, M. (2021). The importance of size and location within gregarious populations of *Ernietta plateauensis*. *Front. Earth Sci.* **9**, 749150.
61. Etminan, V., Lowe, R.J., and Ghisalberti, M. (2017). A new model for predicting the drag exerted by vegetation canopies. *Water Resour. Res.* **53**, 3179–3196.
62. Wickham, H., François, R., Henry, L., Müller, K., and Vaughan, D. (2023). dplyr: a grammar of data manipulation. <https://dplyr.tidyverse.org>. <https://github.com/tidyverse/dplyr>.
63. Welch, B.L. (1947). The generalization of ‘Student’s’ problem when several different population variances are involved. *Biometrika* **34**, 28–35.
64. Ansari, A.R., and Bradley, R.A. (1960). Rank-sum tests for dispersions. *Ann. Math. Statist.* **31**, 1174–1189.
65. Shapiro, S.S., and Wilk, M.B. (1965). An analysis of variance test for normality (complete samples). *Biometrika* **52**, 591–611.
66. Wickham, H. (2016). ggplot2. *Elegant Graphics for Data Analysis* (Springer).

## STAR★METHODS

### KEY RESOURCES TABLE

REAGENT or RESOURCE	SOURCE	IDENTIFIER
<b>Deposited data</b>		
Details of simulated communities	This paper	Zenodo: <a href="http://www.doi.org/10.5281/zenodo.11001479">http://www.doi.org/10.5281/zenodo.11001479</a>
Digital models of Ediacaran organisms	This paper	Zenodo: <a href="http://www.doi.org/10.5281/zenodo.11001479">http://www.doi.org/10.5281/zenodo.11001479</a>
Digital model of extant coral	Pomeroy et al. <sup>46</sup>	Zenodo: <a href="http://www.doi.org/10.5281/zenodo.4281962">http://www.doi.org/10.5281/zenodo.4281962</a>
CFD results files	This paper	Zenodo: <a href="http://www.doi.org/10.5281/zenodo.11001479">http://www.doi.org/10.5281/zenodo.11001479</a>
<b>Software and algorithms</b>		
R	R Core Team <sup>47</sup>	<a href="https://www.R-project.org">https://www.R-project.org</a>
Rhinoceros 3D v. 7	Robert McNeel & Associates	<a href="https://www.rhino3d.com">https://www.rhino3d.com</a>
COMSOL Multiphysics v. 5.6	COMSOL	<a href="https://www.comsol.com">https://www.comsol.com</a>
Geomagic Wrap v. 2021	3D Systems	<a href="https://oqton.com/geomagic-wrap/">https://oqton.com/geomagic-wrap/</a>

### RESOURCE AVAILABILITY

#### Lead contact

Further information and requests for resources should be directed to and will be fulfilled by the lead contact, Imran Rahman ([imran.rahman@nhm.ac.uk](mailto:imran.rahman@nhm.ac.uk)).

#### Materials availability

This study did not generate new materials.

#### Data and code availability

- Spreadsheets and text files with details of the simulated communities, digital models and CFD results files are available at Zenodo: <http://www.doi.org/10.5281/zenodo.11001479>.
- The code used for spatial ecological modelling is available at GitHub: <https://github.com/egmitchell/SpatialSimulations>.
- Any additional information required to reanalyze the data reported in this paper is available from the lead contact upon request.

### EXPERIMENTAL MODEL AND SUBJECT DETAILS

#### Material

We analyzed three *in situ* bedding surfaces of the Avalon assemblage in Mistaken Point, Newfoundland, Canada: the 'D', 'E', and Lower Mistaken Point (LMP) surfaces.<sup>8,14–16</sup> These surfaces are interpreted as turbidite beds deposited in deep marine settings,<sup>14,48</sup> with fossil specimens preserved as molds under beds of volcanic ash.

### METHOD DETAILS

#### Digital modeling of virtual communities

We used the package spatstat<sup>19</sup> in R<sup>47</sup> to simulate five 1 m<sup>2</sup> virtual communities for each of the D, E, and LMP surfaces, in which size, density, spatial distribution, and orientation were based on data compiled for those three surfaces.<sup>9,16–18</sup> The spatial distribution of taxa in these simulated communities accounted for previously identified intra and interspecific interactions,<sup>9,16,18</sup> with complete spatial randomness modelled by homogeneous Poisson models, habitat heterogeneities by heterogeneous Poisson models and reproductive processes by Thomas Cluster models (<https://github.com/egmitchell/SpatialSimulations>).

Three-dimensional digital models of the most abundant organisms on these three surfaces were produced using the computer-aided design program Rhinoceros 3D version 7 ([www.rhino3d.com](http://www.rhino3d.com)) (Figure S1A). Non-uniform rational basis spline (NURBS) models were created based on photographs and detailed observations of well-preserved specimens and published reconstructions. Modelled taxa included: *Pectinifrons abyssalis*<sup>40,49</sup> for the D surface; *Fractofusus misrai*<sup>50</sup> and *Bradgatia linfordensis*<sup>51</sup> for the D and E surfaces; *Primocandelabrum* sp.,<sup>52</sup> *Plumeropriscum hofmanni*,<sup>53</sup> *Thectardis avalonensis*,<sup>54</sup> and *Charniodiscus procerus*<sup>55</sup> for the E surface; *Charniodiscus spinosus*<sup>55</sup> and *Beothukis mistakensis*<sup>56</sup> for the E and LMP surfaces; and *Culmofrons plumosa*,<sup>56</sup>

‘ostrich feather’,<sup>8</sup> and a generic frond for the LMP surface. These simple, idealized models encapsulated the general morphology of each taxon based on the most widely accepted interpretations of known fossil evidence. Details such as individual fronds or frondlets and fractal branching were omitted to economize on computational resources.

Three-dimensional virtual communities were created in Rhinoceros 3D, with digital models of organisms arranged over a 1 m<sup>2</sup> surface based on the coordinates generated in R (Figure S1B). Dimensions and orientation were specified for each individual model. The height of *Fractofusus* individuals, which is not preserved in any fossils, was modelled as a quarter of the width, assuming this taxon was formed of two vanes.<sup>18</sup> Frondose taxa were modelled with the frond upright and orientated perpendicular to flow, consistent with fossils showing a strong preferred orientation, suggestive of alignment to currents.<sup>14,48,57</sup> *Fractofusus* and *Pectinifrons* had their major axes orientated randomly to flow, based on the lack of preferred orientation observed in fossils.<sup>49,57</sup> Finally, *Bradgatia* and *Thectardis* were modelled as radially symmetrical and thus did not require orientating. Where necessary, models were repositioned randomly (on the D surface) or slightly shifted while remaining in contact with their xy coordinate (on the E and LMP surfaces) to avoid overlap. The final virtual communities were exported in .STP format.

The frontal area index ( $\lambda$ ), a measure of the canopy density commonly used to predict the behavior of the canopy flow,<sup>7,22,24</sup> was calculated for each virtual community as the element planform area per unit of community surface:

$$\lambda = \frac{A}{S}$$

where  $A$  is the total planform area of all organisms exposed to the flow and  $S$  is the surface area of each community (1 m<sup>2</sup>). We obtained the total frontal planform areas by projecting model geometries onto a plane perpendicular to flow with the ‘ProjectToCPlane’ function and subsequently measured them using the ‘Area’ tool in Rhino. Additionally, we calculated the height-based distinct vertical stratification (DVS<sup>height</sup>), defined as the fraction of specimens from each taxon that did not belong to the same 1 cm height bin as any specimens from a different taxon on the same surface, as a measurement of tiering for each simulated community, following Mitchell & Kenchington<sup>18</sup> (see their supplementary figure 2).

### Computational fluid dynamics

Computational fluid dynamics (CFD) simulations of water flow were carried out using the software COMSOL Multiphysics version 5.6 ([www.comsol.com](http://www.comsol.com)). The computational domain consisted of a hexahedron measuring 3 m in length and 1.2 m in width. The height was calculated as 3× the height of the tallest individual, with a minimum height of 48 cm, which in all cases produced domains more than ten times the average community height and thus were sufficiently tall to enable canopy flow to develop.<sup>7</sup> An additional cuboid, 1.5× the height of the tallest individual, was created over the 1 m<sup>2</sup> surface to define a volume of mesh refinement closest to the organisms. We then assigned boundary conditions to the flow domain. All boundaries where fluid–solid interactions occurred, including the lower face of the hexahedron, which represents the seafloor, and the walls of the organisms, were prescribed a no-slip boundary condition. A ‘fully developed’ inlet velocity boundary condition was prescribed at the upstream end of the hexahedron where flow entered the domain and a zero-pressure boundary outlet condition with back-flow suppression was specified at the opposing end. We prescribed periodic flow boundaries at the sides of the domain with a 0 Pa pressure differential to avoid instabilities of the flow that can result in poor convergence, and a slip boundary condition at the top of the domain. Standard material properties for liquid water (density  $\rho = 1000$  kg/m<sup>3</sup>, dynamic viscosity  $\mu = 0.001$  kg/s·m) were assigned to the flow domain.

Fossiliferous surfaces from Mistaken Point are interpreted as having been deposited in deep marine environments, influenced by contour currents, at depths below the photic zone.<sup>14,48</sup> We constrained the simulated inlet velocities based on inferences from palaeo-current data. The sediment grain size and bedforms described for these Mistaken Point surfaces<sup>14</sup> are suggestive of flow velocities between 0.01 and 0.2 m/s, according to the bedform-velocity matrix of Stow et al.,<sup>58</sup> consistent with current velocities previously inferred for these surfaces.<sup>10</sup> We performed CFD simulations at four inlet velocities within this range (0.01, 0.05, 0.1, and 0.2 m/s), resulting in Reynolds numbers (Re) ranging from 9960 to 99600 (based on the community area length of 1 m). Three-dimensional, incompressible flow was simulated using a turbulent closure, consistent with the marine benthic boundary layer, which is naturally turbulent even at low flow velocities.<sup>10</sup> A stationary solver was used to compute the Reynolds averaged Navier-Stokes (RANS) equations using the Spalart-Allmaras (SA) one-equation eddy viscosity model,<sup>59</sup> a robust turbulence closure with an optimal performance at adverse pressure gradients. The Spalart-Allmaras (SA) model provides results virtually identical to those of the more complex RANS turbulence models such as the shear stress transport SST (see below), but shows better convergence and uses fewer computational resources, and has been previously applied to study flow patterns in idealized populations of the Ediacaran organism *Ernieia plateauensis*.<sup>60</sup>

The flow domain was meshed using a mixture of unstructured and structured meshes. Unstructured tetrahedral meshes were used for the free-flow areas, with six layers of prismatic elements used along the no-slip boundaries. We created an area of extra refinement in the vicinity of the organisms, where the mesh size was smaller than in the more distant parts of the domain, to provide good resolution for simulating the wakes of organisms and their potential interactions. Four meshes with increasingly small elements were tested for one simulated community at an inlet velocity of 0.1 m/s. We monitored flow velocity profiles at 10 random coordinates throughout the community, and selected the mesh where profiles did not change substantially with increasing refinement. To evaluate this, we obtained  $U$  velocity profiles from  $z = 0$  to  $z = 40$  cm and calculated the area underneath each curve. A combination of COMSOL’s pre-defined ‘fine’ element size (maximum element size = 4.9 mm, minimum element size = 1.47 mm, maximum element growth rate = 1.2, curvature factor = 0.7, resolution of narrow regions = 0.6) in the far field and ‘extra-fine’ (maximum element size = 1.81, minimum



element size = 0.196, maximum element growth rate = 1.1, curvature factor = 0.4, resolution of narrow regions = 0.9) in the refinement box was found to produce mesh independent velocity profiles, i.e., velocity curves less than 2% different than those of the immediately coarser mesh, and this mesh ('mesh 1') was selected for use in all subsequent analyses. We also tested the sensitivity of the results to variations in domain size and turbulence models. This confirmed our results were largely independent of domain size and showed that the Spalart Allmaras model produced results virtually identical to those obtained with more complex RANS turbulence models, while giving better convergence and using fewer computational resources.

### Sensitivity tests

For comparison with the simulated Ediacaran communities, we assembled an idealized virtual coral reef. This virtual community was composed of multiple closely-spaced colonies of the extant table-shaped coral *Acropora hyacinthus*. We converted a digital model of *A. hyacinthus* from Pomeroy et al.<sup>46</sup> into a NURBS surface using the auto-surfacing tools in Geomagic Wrap version 2021 ([www.oqton.com/geomagic-wrap](http://www.oqton.com/geomagic-wrap)), which was then exported in .IGES format. This model was imported into COMSOL and duplicated to give a total of 25 models, which were arranged over a 1m<sup>2</sup> surface to give a coverage of ~20%. Following Pomeroy et al.,<sup>46</sup> model size and spacing were kept constant, which is considered an appropriate simplification when evaluating results across the entire canopy.<sup>46,61</sup> This virtual community was then used in a CFD simulation performed in COMSOL using the same settings as the main analyses, with an inlet velocity of 0.1 m/s.

We also examined the sensitivity of our results to different reconstructions of *Bradgatia*. *Bradgatia* is interpreted as being composed of eight primary fronds arranged around a central branching point, with four taphomorphs (I, V, U, O) distinguished based on the spread of the fronds.<sup>51</sup> For our main analyses, we modelled *Bradgatia* with the general shape of the head of a Boston lettuce, the inferred three-dimensional shape of the U-shaped taphomorphs present on the D and E surfaces. As part of our sensitivity tests, we produced an alternative model with a more compact shape ('compact'). This resembles the head of a Romaine lettuce, with a narrower diameter and the absence of a middle cavity, which resulted from the tighter primary fronds. In addition, we constructed a model with narrow gaps between the eight primary fronds ('gappy'). All the simulated community arrangements for the D and E surfaces were repeated by substituting our original model of *Bradgatia* with the alternative 'compact' and 'gappy' models, and these were then used in CFD simulations performed with the same settings as the main analyses.

### QUANTIFICATION AND STATISTICAL ANALYSIS

Vertical ( $w$ ) and lateral ( $v$ ) velocity components were sampled from a point grid covering the 1 m<sup>2</sup> community and reaching a height of  $z = 30$  cm. This grid was formed by 20 evenly spaced points along the  $x$ ,  $y$ , and  $z$  coordinates. Streamwise velocity ( $u$ ) was sampled from 20 evenly spaced lines at the end of the domain,  $x = 100$  cm, where each line was made of 60 log<sub>10</sub> distributed points from  $z = 0$  to  $z = 30$  cm. Streamwise velocity ( $u$ ) profiles from the undisturbed boundary layer were sampled from a line at a central point at the inlet.

The standard deviation (SD) of these two velocity components was calculated for each simulation using the `summarize` function of the package `dplyr`<sup>62</sup> in R.<sup>47</sup> Pairwise comparisons of the standard deviation between surfaces ( $n = 5$  per group) were performed using Welch's  $t$ -test,<sup>63</sup> which compares the means of the standard deviations, assuming a normal distribution and unequal variances. Equality of variances and normality tests were performed per group prior to applying the  $t$ -test using the Ansari-Bradley<sup>64</sup> test and the Shapiro-Wilk normality test,<sup>65</sup> respectively. All graphs were made using the graphic R package `ggplot2`.<sup>66</sup>

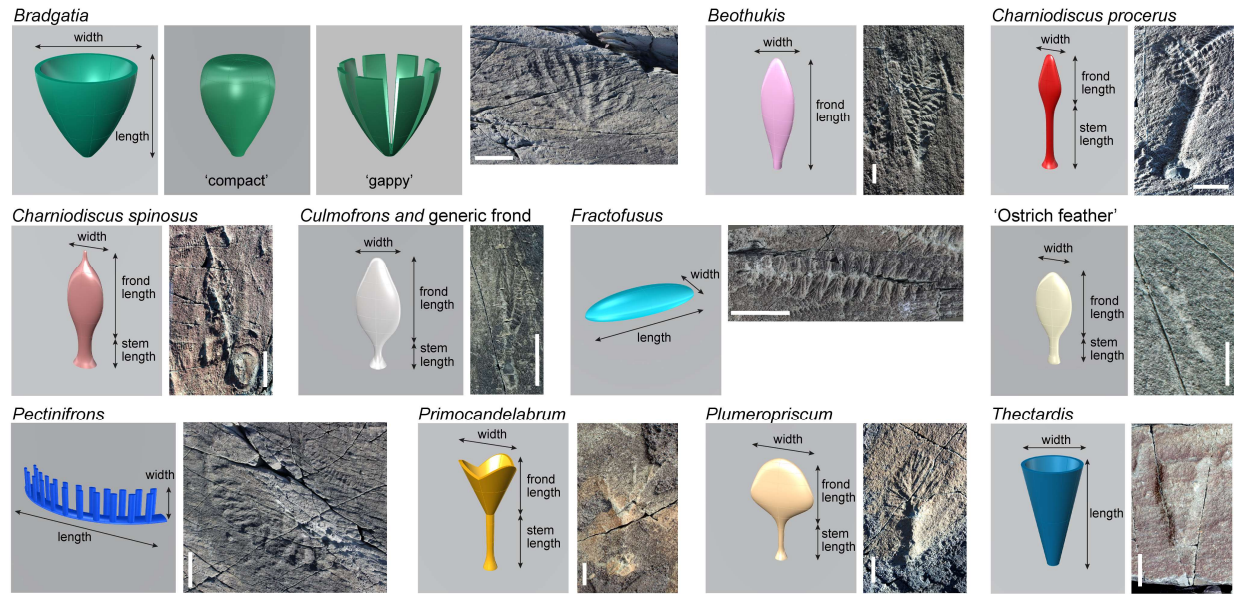
**Current Biology, Volume 34**

**Supplemental Information**

**Ediacaran marine animal forests  
and the ventilation of the oceans**

**Susana Gutarra, Emily G. Mitchell, Frances S. Dunn, Brandt M. Gibson, Rachel A. Racicot, Simon A.F. Darroch, and Imran A. Rahman**

**A**



**B**

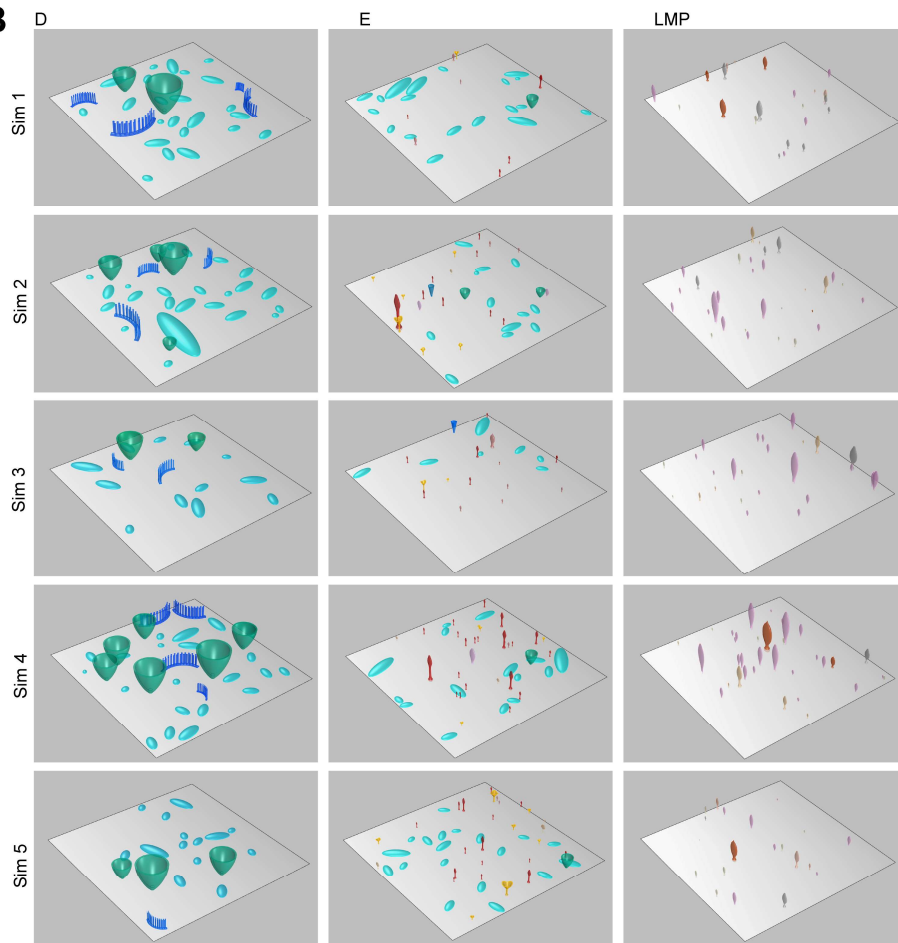


**Figure S1. Digital three-dimensional models and fossil specimens of the main organisms from the D, E, and LMP surfaces. Related to Figures 1, 2, and 3.**



(A) Digital models in oblique view (not to scale), showing the dimensions specified in the community simulations, adjacent to the corresponding fossil specimens. Fossils of *Fractofusus*, *Pectinifrons*, and *Bradgatia* from the D surface. Fossils of *Charniodiscus procerus*, *Charniodiscus spinosus*, *Thectardis*, *Primocandelabrum*, *Plumeropriscum*, and *Beothukis* from the E surface. Fossils of ‘ostrich feather’ and *Culmofrons* from the LMP surface. Scale bars equal 2 cm (*Fractofusus*, *Pectinifrons*, *Bradgatia*, *Thectardis*, *Primocandelabrum*, *Plumeropriscum*, ‘ostrich feather’, *Beothukis*) or 5 cm (*Charniodiscus procerus*, *Charniodiscus spinosus*, *Culmofrons*).

(B) Five simulated communities (Sim 1–Sim 5) of the D, E, and LMP surfaces (1 m<sup>2</sup> area).

Oblique views showing organisms in 3-D.

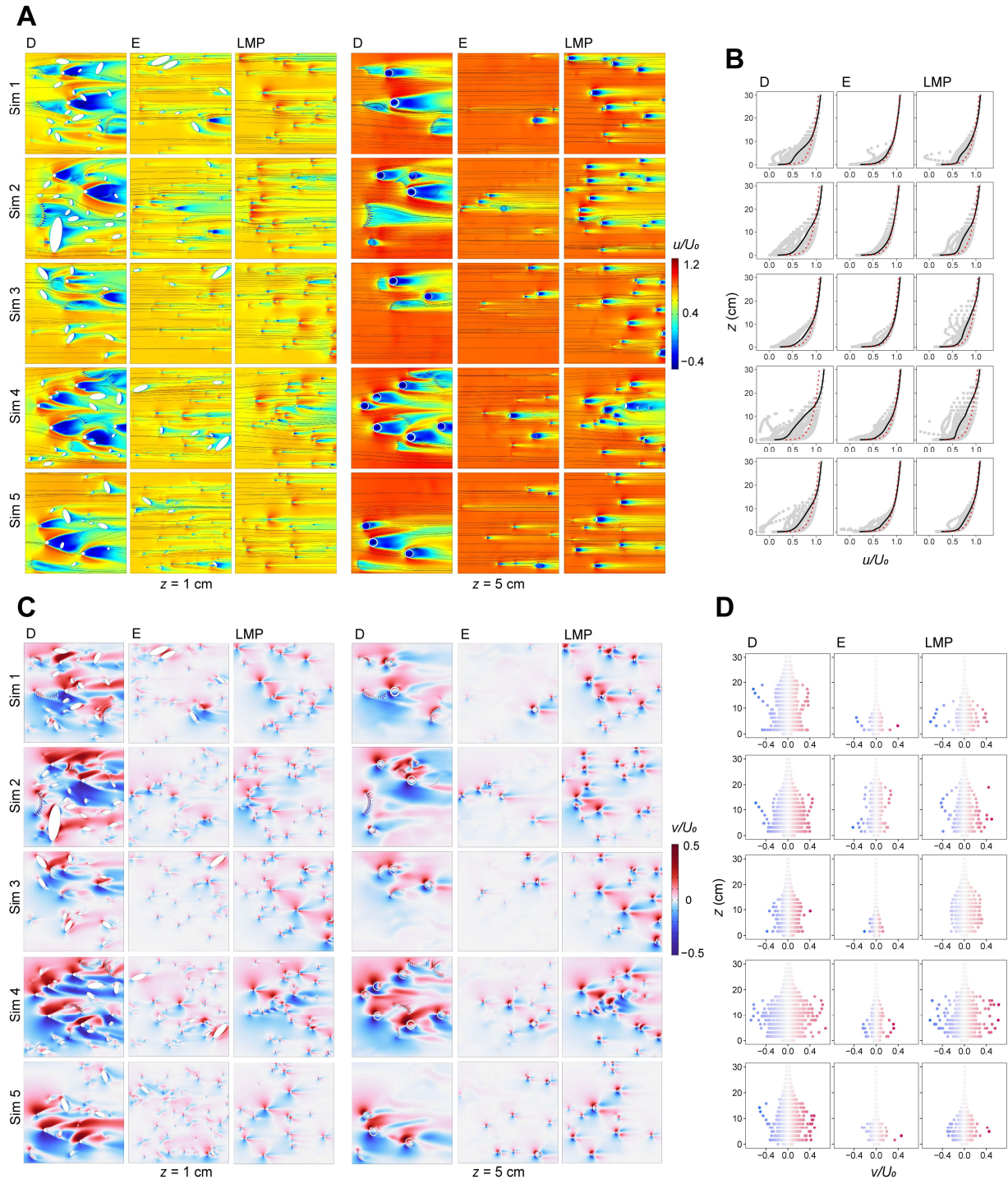


**Figure S2. Flow patterns for virtual communities of three Mistaken Point assemblages.**

**Related to Figures 1 and 2.**

(A, B) Streamwise velocity plots. (A) CFD results for five simulated communities (Sim 1–Sim 5) of the D, E, and LMP surfaces. Two-dimensional plots of streamwise velocity ( $u$ ) relative to the inlet velocity ( $U_0 = 0.1 \text{ m s}^{-1}$ ) for two horizontal cross-sections at heights  $z = 1 \text{ cm}$  (left

panel) and  $z = 5$  cm (central panel). Direction of ambient flow from left to right. (B) Plots of streamwise velocity ( $u$ ) relative to the inlet velocity ( $U_0 = 0.1 \text{ m s}^{-1}$ ) at heights between  $z = 0$  to  $z = 30$  cm. The black line shows the mean velocity and the dotted red line shows an undisturbed boundary layer profile. Velocity measured at the back of the community.

(C, D) Lateral velocity plots. (C) CFD results for five simulated communities (Sim 1–Sim 5) of the D, E, and LMP surfaces. Two-dimensional plots of lateral velocity ( $v$ ) relative to the inlet velocity ( $U_0 = 0.1 \text{ m s}^{-1}$ ) for two horizontal cross-sections at heights  $z = 1$  cm (left panel) and  $z = 5$  cm (central panel). Direction of ambient flow from left to right. (D) Plots of lateral velocity ( $v$ ) relative to the inlet velocity ( $U_0 = 0.1 \text{ m s}^{-1}$ ) at heights between  $z = 0$  to  $z = 30$  cm. Velocity sampled from a grid of  $20 \times 20 \times 20$  points in  $x$ ,  $y$ , and  $z$  directions over the  $1 \text{ m}^2$  community.



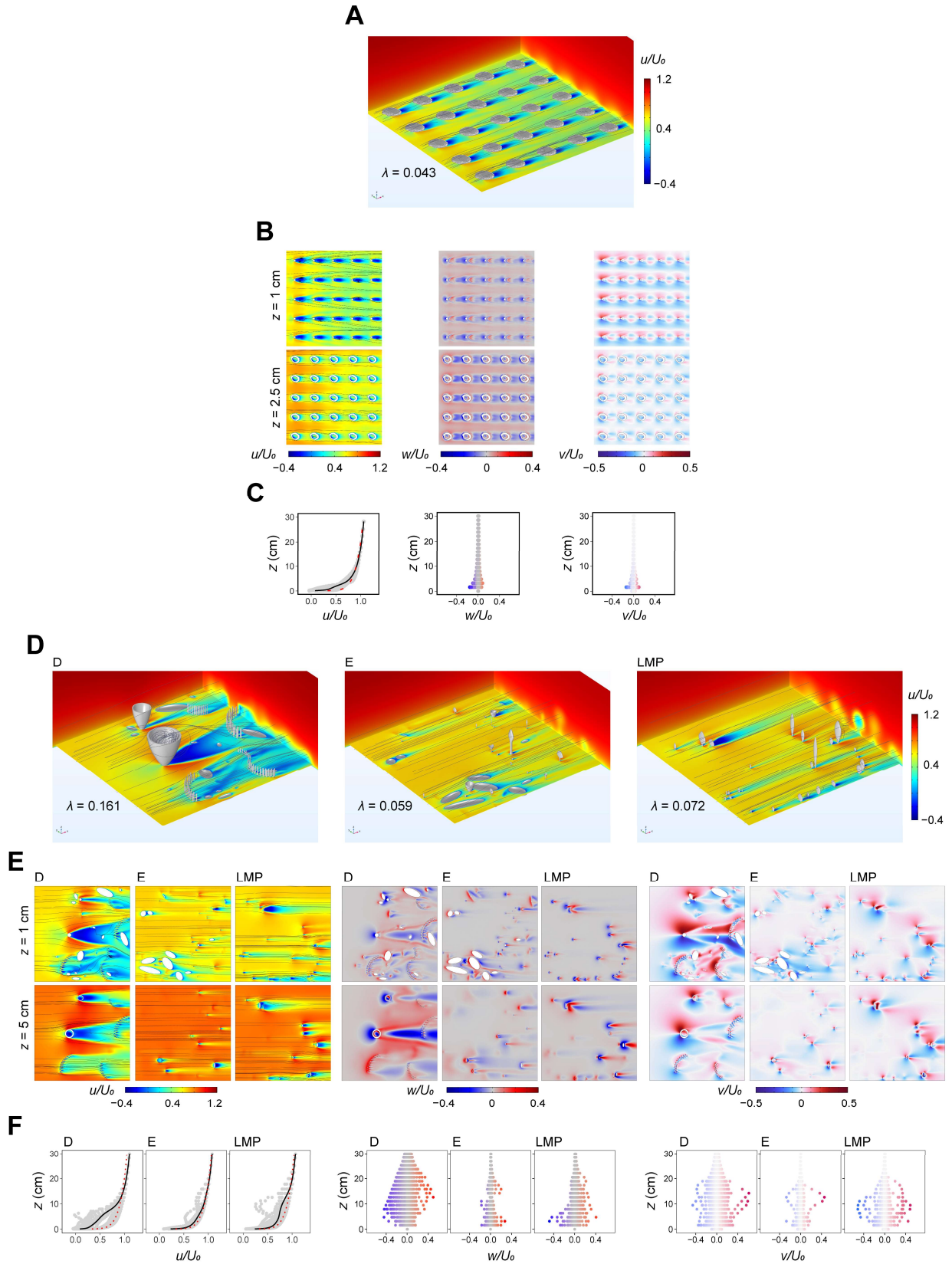


**Figure S3. Flow patterns from virtual coral reef and quadrants of three Mistaken Point assemblages. Related to Figures 1, 2, and 3.**

(A–C) Virtual coral reef. (A) Oblique view showing organisms in 3-D, flow streamlines (grey lines), and two-dimensional plots of the streamwise velocity (at height  $z = 1$  cm in the horizontal plane and two vertical planes). The frontal area index ( $\lambda$ ) is shown. (B) Two-dimensional plots of streamwise ( $u$ , left panel), vertical ( $w$ , central panel), and lateral ( $v$ , right panel) velocity relative to the inlet velocity ( $U_0 = 0.1 \text{ m s}^{-1}$ ) for two horizontal cross-sections at heights  $z = 1$  cm and  $z = 2.5$  cm. (C) Plots of normalised streamwise velocity (left panel, black line shows mean velocity, dotted red line shows undisturbed boundary layer profile at inlet), vertical velocity (central panel), and lateral velocity (right panel) at heights between  $z = 0$  to  $z = 30$  cm. Streamwise velocity was measured at the back of the community. Vertical and lateral velocities were sampled from a grid of  $20 \times 20 \times 20$  points in  $x$ ,  $y$ , and  $z$  directions over the  $1 \text{ m}^2$  community.

(D–F) CFD results for randomly sampled  $1 \text{ m}^2$  quadrants of the D, E, and LMP surfaces (D6, C4, and H8, respectively, from Mitchell & Kenchington<sup>S1</sup>). (D) Oblique views showing organisms in 3-D, flow streamlines (grey lines), and two-dimensional plots of the streamwise velocity (at height  $z = 1$  cm in the horizontal plane and two vertical planes). The frontal area index ( $\lambda$ ) is shown for each quadrant. (E) Two-dimensional plots of streamwise ( $u$ , left panel), vertical ( $w$ , central panel), and lateral ( $v$ , right panel) velocity relative to the inlet velocity ( $U_0 = 0.1 \text{ m s}^{-1}$ ) for two horizontal cross-sections at heights  $z = 1$  cm and  $z = 5$  cm. (F) Plots of normalised streamwise velocity (left panel, black line shows mean velocity, dotted red line shows undisturbed boundary layer profile at inlet), vertical velocity (central panel), and lateral velocity (right panel) at heights between  $z = 0$  to  $z = 30$  cm. Streamwise velocity was measured at the back of the community. Vertical and lateral velocities were sampled from a grid of  $20 \times 20 \times 20$  points in  $x$ ,  $y$ , and  $z$  directions over the  $1 \text{ m}^2$  community.

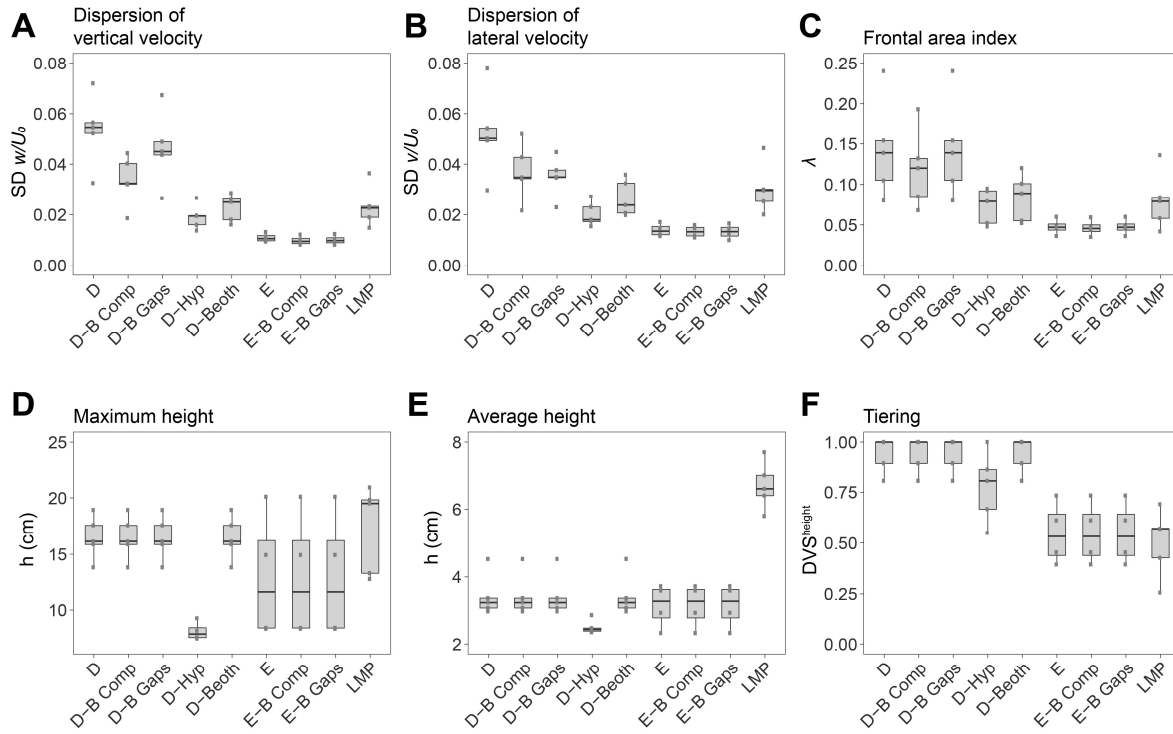


**Figure S4. Sensitivity tests of *Bradgatia* morphology and community structure and composition. Related to Figure 4.**

Comparison of vertical and lateral velocity dispersion and geometrical parameters for the five original simulated communities of the D, E, and LMP surfaces and alternative simulations of the D and E surfaces with ‘compact’ (D–B Comp and E–B Comp) and ‘gappy’ (D–B Gaps and E–B Gaps) *Bradgatia* models, with *Bradgatia* re-sized to match the height distribution on the E surface (D–Hyp), and with *Bradgatia* replaced by *Beothukis* (D–Beoth).

(A, B) Standard deviation (SD) of the vertical (A) and lateral (B) velocity components ( $w$  and  $v$ , respectively, normalised to the inlet velocity of  $U_0 = 0.1 \text{ m s}^{-1}$ ).

(C) Frontal area index ( $\lambda$ ) calculated as the element planform area per unit of community area.

(D) Maximum height ( $h$ ) represented by the height of the tallest organism in each community.

(E) Average height ( $h$ ) calculated as the average height of all organisms in each community.

(F) Tiering metric, indicating the degree of distinct vertical stratification based on total height ( $\text{DVS}^{\text{height}}$ ). Box plots display individual values (grey points), median (black line), and

interquartile range (grey box).

	SD Vertical velocity		SD Lateral velocity	
D vs E	<b>0.0022</b>	**	<b>0.0057</b>	**
D vs LMP	<b>0.0051</b>	**	<b>0.0458</b>	*
E vs LMP	<b>0.0229</b>	*	<b>0.0124</b>	*
D vs D-Hyp	<b>0.0037</b>	**	<b>0.0120</b>	*
D vs D-Beoth	<b>0.0056</b>	**	<b>0.0249</b>	*
D vs D Brad 'compact'	<b>0.0345</b>	*	0.1427	NS
E vs E Brad 'compact'	0.3952	NS	0.7388	NS
D Brad 'compact' vs E Brad 'compact'	<b>0.0050</b>	**	<b>0.0078</b>	**
D Brad 'compact' vs LMP	0.1099	NS	0.3412	NS
E Brad 'compact' vs LMP	<b>0.0186</b>	*	<b>0.0164</b>	*
D vs D Brad 'gaps'	0.4427	NS	0.0968	NS
E vs E Brad 'gaps'	0.5045	NS	0.7441	NS
D Brad 'gaps' vs E Brad 'gaps'	<b>0.0018</b>	**	<b>0.0013</b>	**
D Brad 'gaps' vs LMP	<b>0.0148</b>	*	0.4322	NS
E Brad 'gaps' vs LMP	<b>0.0158</b>	*	<b>0.0131</b>	*

**Table S1. *p*-values from pairwise comparisons of vertical and lateral velocity dispersion for virtual communities of three Mistaken Point assemblages. Related to Figure 4.**

Results of Welch's two-sample *t*-test comparing the standard deviation between the original simulated communities ( $n = 5$  per group) of the D, E, and LMP surfaces, plus alternative simulations with D surface *Bradgatia* re-sized to match the height distribution on the E surface (D-Hyp) or replaced by *Beothukis* (D-Beoth) and with alternative 'compact' (D Brad 'compact' and E Brad 'compact') and 'gappy' (D Brad 'gaps' and E Brad 'gaps') *Bradgatia* models ( $n = 4$  or  $5$  per group). Statistically significant results highlighted in bold. Significance level denoted by asterisks and lack of significance by NS.



D							% Frontal area per taxon		
		ind/ m <sup>2</sup>	max h (cm)	avg h (cm)	$\lambda$	Tiering Metric	<i>Fractofusus</i>	<i>Bradgatia</i>	<i>Pectinifrons</i>
D	Sim1	29	18.93	2.96	0.139	1	25.48%	51.96%	22.56%
D	Sim2	30	16.14	3.06	0.154	0.805556	29.94%	49.47%	20.59%
D	Sim3	16	13.83	3.22	0.080	1	31.02%	50.65%	18.33%
D	Sim4	30	17.57	4.52	0.240	0.895833	11.43%	73.11%	15.46%
D	Sim5	18	15.86	3.38	0.105	1	22.47%	69.74%	7.78%
D	D6 quad	26	18.90	3.27	0.161	1	18.09%	42.84%	39.07%
	Average	24.6	16.5	3.4	0.144	0.950	23.07%	56.29%	20.63%

E							% Frontal area per taxon							
		ind/ m <sup>2</sup>	max h (cm)	avg h (cm)	$\lambda$	Tiering Metric	<i>Fractofusus</i>	<i>Bradgatia</i>	<i>Charniodiscus procerus</i>	<i>Charniodiscus spinosus</i>	<i>Beothukis</i>	<i>Prinocandela -brum</i>	<i>Plumeropris- cum</i>	<i>Thectardis</i>
E	Sim1	28	8.36	2.32	0.036	0.733333	64.52%	17.07%	9.05%	7.89%	0.00%	1.47%	0.00%	0.00%
E	Sim2	34	20.1	3.6	0.046	0.453125	27.37%	15.86%	30.34%	2.42%	0.00%	6.34%	1.56%	0.00%
E	Sim3	22	8.88	3.32	0.024	0.774286	38.63%	0.00%	17.94%	24.58%	0.00%	4.57%	0.00%	14.27%
E	Sim4	45	14.92	3.722	0.060	0.611905	36.17%	10.92%	37.78%	1.54%	10.27%	1.09%	2.23%	0.00%
E	Sim5	47	8.44	2.92	0.048	0.393651	44.57%	12.37%	23.10%	1.56%	0.00%	12.32%	6.08%	0.00%
E	C4 quad	49	16.7	2.6	0.059	0.52	55.59%	9.65%	17.69%	1.12%	0.00%	3.01%	12.93%	0.00%
	Average	35.2	12.1	3.2	0.043	0.581	44.47%	10.98%	22.65%	6.52%	1.71%	4.80%	3.80%	2.38%

LMP							% Frontal area per taxon				
		ind/ m <sup>2</sup>	max h (cm)	avg h (cm)	$\lambda$	Tiering Metric	<i>Beothukis</i>	<i>Culmofrons</i>	Ostrich feather	<i>Charniodiscus procerus</i>	Generic frond
LMP	Sim1	22	13.32	6.6	0.058	0.570952	21.98%	8.39%	5.97%	27.48%	36.18%
LMP	Sim2	30	19.51	6.4	0.079	0.426667	64.41%	12.51%	7.79%	0.21%	15.08%
LMP	Sim3	26	19.83	7	0.084	0.691176	74.96%	8.63%	3.82%	0.00%	12.59%
LMP	Sim4	34	20.92	7.7	0.136	0.256364	70.38%	7.96%	2.27%	2.27%	3.09%
LMP	Sim5	20	12.81	5.8	0.042	0.571429	32.19%	18.11%	17.04%	22.06%	10.60%
LMP	H8	28	20.2	5.9	0.072	0.399	65.35%	11.95%	6.08%	5.15%	11.47%
	Average	26.7	17.8	6.6	0.079	0.486	54.88%	11.26%	7.16%	9.53%	14.84%

**Table S2. Properties of virtual communities of three Mistaken Point assemblages. Related to Figure 4.**

Abbreviations: avg, average; h, height; ind, individuals; max, maximum;  $\lambda$ , frontal area index.

## **SUPPLEMENTARY REFERENCE**

- S1. Mitchell, E.G., and Kenchington, C.G. (2018). The utility of height for the Ediacaran organisms of Mistaken Point. *Nat. Ecol. Evol.* 2, 1218–1222.